applied sciences

MDPI

Article

An Integrated Data-Driven Predictive Resilience Framework for Disaster Evacuation Traffic Management

Tanzina Afrin [1,*], Lucy G. Aragon [2], Zhibin Lin [3] and Nita Yodo [1,3,*]

[1] Department of Industrial and Manufacturing Engineering, North Dakota State University, Fargo, ND 58102, USA
[2] Department of Engineering, Pontifical Catholic University of Peru, Lima 15088, Peru
[3] Department of Civil, Construction, and Environmental Engineering, North Dakota State University, Fargo, ND 58102, USA
* Correspondence: tanzina.afrin@ndsu.edu (T.A.); nita.yodo@ndsu.edu (N.Y.)

Abstract: Maintaining smooth traffic during disaster evacuation is a lifesaving step. Traffic resilience is often used to define the ability of a roadway during disaster evacuation to withstand and recover its functionality from disturbances in terms of traffic flow caused by a disaster. However, a high level of variances due to system complexity and inherent uncertainty associated with disaster and evacuation risks poses great challenges in predicting traffic resilience during evacuation. To fill this gap, this study aimed to propose a new integrated data-driven predictive resilience framework that enables incorporating traffic uncertainty factors in determining road traffic conditions and predicting traffic performance using machine learning approaches and various space and time (spatiotemporal) data sources. This study employed an augmented Long Short-Term Memory (LSTM)-based approach with correlated spatiotemporal traffic data to predict traffic conditions, then to map those conditions to traffic resilience levels: daily traffic, segment traffic, and overall route traffic. A case study of Hurricane Irma's evacuation traffic was used to demonstrate the effectiveness of the proposed framework. The results indicated that the proposed method could effectively predict traffic conditions and thus help to determine traffic resilience. The data also confirmed that the traffic infrastructures along the US I-75 route remained resilient despite the disturbances during the disaster evacuation activities. The findings of this study suggest that the proposed framework is applicable to other disaster management scenarios to obtain more robust decisions for the emergency response during disaster evacuation.

Keywords: resilience; data-driven; LSTM; traffic; transportation; disaster; management; evacuation

Citation: Afrin, T.; Aragon, L.G.; Lin, Z.; Yodo, N. An Integrated Data-Driven Predictive Resilience Framework for Disaster Evacuation Traffic Management. *Appl. Sci.* **2023**, *13*, 6850. https://doi.org/10.3390/app13116850

Academic Editor: Luís Picado Santos

Received: 1 April 2023
Revised: 27 May 2023
Accepted: 3 June 2023
Published: 5 June 2023

1. Introduction

The aftermath of natural hazard occurrences such as hurricanes, landslides, blizzards, or wildfires poses inevitable social, economic, and environmental disruptions. The National Research Council defines disaster management as efforts to reduce the impact of disasters encompassing four stages: mitigation, preparedness, response, and recovery [1]. Transportation infrastructure is very crucial in the four stages of disaster management [2]. During the mitigation stage, transportation infrastructure reduces or eliminates risk to disaster victims by providing evacuation means to retreat from hazards and their effects [3]. In the preparedness and response stage, transportation infrastructure should accommodate the efficient response of emergency personnel to combat threats, save lives, and preserve property [4]. After the adverse impacts have passed, transportation infrastructure is the connection for the humanitarian aid responders, the victims, and other volunteers to work together to stabilize the community in the recovery stage [5].

Although it is expected that the road network be constantly operational and efficient during disaster management, the transportation infrastructure itself is vulnerable to disaster [6]. In the mitigation stage, the rapidly increased car volume to roadway capacity ratio

and dynamic decisions from emergency responses often result in traffic congestion during evacuation [7]. This type of traffic congestion is known as non-recurring congestion, which can be potentially life-threatening if the impact of hazards increases in scale or changes in direction [8]. Thus, it is necessary to ensure efficient traffic flows during a hectic period of disaster evacuation to ensure a successful implementation of evacuation with minimal time and disaster casualties. This also translates to the requirement for traffic systems to be resilient.

A resilient traffic system can manage disaster impacts by maintaining traffic operability pre-, during, and post-disaster, and by recovering from traffic disruptions [4]. Traffic resilience is often associated with road network conditions. Nogal et al., 2016 developed a dynamic equilibrium-restricted assignment model to evaluate the resilience of a road network [9]. Calvert and Snelder, 2018 proposed a Link Performance Index for Resilience (LPIR) with robustness and vulnerability concepts to evaluate the resilience level of road sections [10]. Many researchers have worked toward advances in traffic systems to enable resilience concepts in the existing transportation infrastructure. Zhang et al., 2021 incorporated the spatiotemporal property into traffic resilience dynamics in a destination choice model for evacuation applications [11]. Abudayyeh et al., 2021 optimized traffic signals with a semi-automatic cross-entropy optimization method to improve resilience in a disrupted road network [12]. Yao and Chen, 2022 proposed an adaptive traffic signal control strategy based on dynamic phase selection coupled with queue length dissipation to improve resilience in intersections against disruptions [13].

With the technological advances in collecting various traffic data, machine learning and data-driven approaches are often employed to predict or analyze traffic situations due to their ability to handle and process various traffic data [14]. Recently, out of various machine learning algorithms, LSTM-based algorithms have been widely proposed to predict different traffic properties during a hurricane evacuation. In their study, Roy et al., 2021 utilized the LSTM neural network and traffic data from Hurricanes Irma and Matthews to accurately predict traffic demand up to 24 h before the evacuation [15]. In addition to predicting traffic demand, Rahman and Hasan, 2018 applied LSTM to short-term traffic speed prediction during evacuation [16]. In their updated work, Rahman and Hasan (2022) also developed a dynamic graph convolution LSTM (DGCN-LSTM) model to analyze the network dynamics during hurricane evacuation [17].

Incorporating uncertainty in the prediction framework is important because it reflects the reality of unpredictable events during evacuations, such as natural disasters and traffic incidents. However, there are many different sources of uncertainty, such as: (1) Data uncertainty. Accurate data is essential to make predictions, but the data may be incomplete or unreliable during a disaster, leading to uncertainty in the prediction model [18]. (2) Model uncertainty. The models used for prediction and evacuation planning are often based on assumptions and simplifications that may not always hold true [18]. (3) Response uncertainty. In a disaster, people's responses to an evacuation order can be unpredictable. Some may choose to evacuate early, while others may delay or refuse to evacuate, leading to uncertainty in the number of people that need to be evacuated and the routes they may take [2]. Failing to account for uncertainty in disaster evacuation traffic management can lead to underestimating the potential risks and not allocating adequate resources to handle the situation [3]. This can result in delayed response times, inefficient evacuation routes, and inadequate allocation of resources such as emergency services, which can ultimately lead to increased casualties and damage [19].

To overcome this gap, the aim of this paper is to propose a new integrated data-driven predictive resilience framework that incorporates traffic uncertainty factors to assess traffic resilience during disaster evacuation. The research objective is to utilize machine learning approaches and spatiotemporal data sources, specifically an augmented LSTM-based approach, to predict traffic conditions and map them to traffic resilience levels, demonstrating the effectiveness of the proposed framework through a case study of Hurricane Irma's evacuation traffic.

LSTM provides a short- and long-term memory component that is useful for predicting a sequential scenario [20]. Before predicting traffic performance, data uncertainty factors are introduced in measuring the current traffic condition. Incorporating uncertainty allows for the development of more robust and adaptive prediction models that can adjust to changing conditions and make more accurate predictions. Then, the augmented LSTM with the Kalman Filter estimation algorithm is employed in the proposed framework to estimate correlated spatiotemporal traffic data. Lastly, various levels of traffic resilience are quantified based on the predicted parameter value obtained from the framework. The proposed integrated data-driven predictive framework for disaster evacuation traffic management will allow the decision-makers to make more informed decisions by considering the uncertainty and potential risks associated with different courses of action.

The contributions of this paper to the infrastructure preservation and resilience community include: (1) integrating uncertainty factors in road traffic performance measures; (2) applying an improved LSTM approach to predicting traffic scenarios; and (3) quantifying traffic resilience with spatiotemporal data. The information presented in this paper is structured as follows. Section 2 introduces the proposed predictive traffic resilience framework by quantifying road conditions, predicting traffic performance under uncertainty, and measuring traffic resilience. Section 3 details the application effort by applying the proposed framework to the Hurricane Irma scenario. Section 4 discusses the broader impacts of the proposed approach and suggests further research directions, and Section 5 concludes the work proposed in this paper.

2. Integrated Predictive Traffic Resilience Framework

Conventional resilience metrics often fall short in predicting and quantifying the traffic resilience of a transportation infrastructure due to the dynamic and sequential properties of traffic data. Additionally, traffic flow becomes more uncertain under extreme weather conditions, which increases disaster risk and introduces other behavioral factors. To address these issues, a data-driven predictive traffic resilience framework is proposed, as shown in Figure 1.

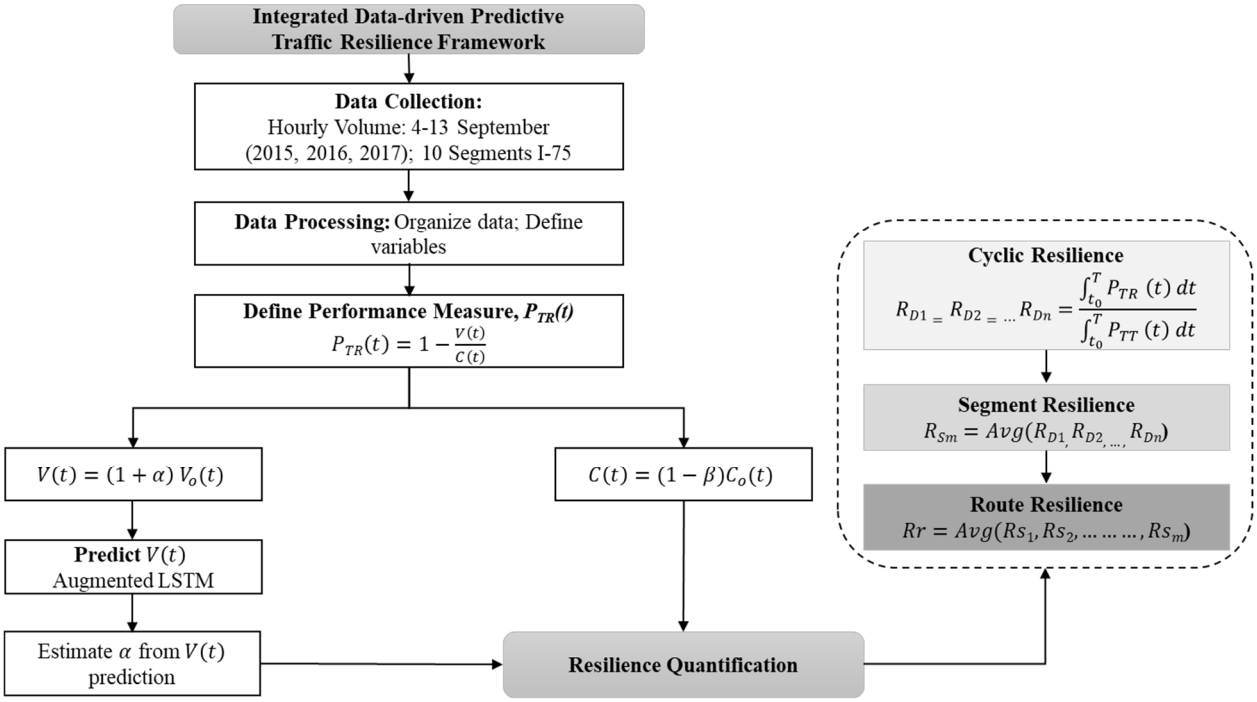

Figure 1. The proposed integrated data-driven predictive traffic resilience framework.

To implement this framework, hourly traffic volume data over a disaster period was collected. In addition, the hourly traffic volume data from the past two years at a

similar time was collected to analyze the change in traffic volume due to the disaster. It should be noted that the hourly traffic volume serves as an index or indicator of traffic resilience rather than directly representing resilience. It is a quantitative measure of traffic volume; by itself, the hourly volume index does not directly reflect the concept of traffic resilience. Traffic resilience refers to the ability of a transportation system to withstand and recover from disruptions or disturbances, such as accidents, congestion, or adverse weather conditions, while maintaining its functionality and performance of free flow or stable flow with unaffected speed.

While the hourly volume can provide valuable information about traffic patterns and congestion levels, it does not capture the broader aspects of traffic resilience. Thus, to quantify traffic resilience, this manuscript also considers additional factors, such as travel time variations based on volume (α) and capacity (β), road network or roadway capacity, alternate route availability (in terms of different segments/routes), and the system's ability to recover from disruptions during the post-adverse events condition. The proposed framework is modeled with a focus on traffic conditions during evacuation before and after any disaster. This proposed integrated framework consists of three main steps: (1) measurement of traffic performance under uncertainty; (2) prediction of the traffic condition with an augmented LSTM-based approach; and (3) quantification of traffic resilience during evacuation. Each of the steps will be detailed as follows.

2.1. Road Traffic Performance under Uncertainty

A variety of traffic condition measures are available and are employed by different transportation departments [7]. In practice, the level of service (LoS) determined by the Highway Capacity Manual (HCM) has become widely adopted in measuring traffic conditions as it accounts for variabilities with peak hour factor (PHF) [21–23]. To determine the LoS of a roadway, the volume-to-capacity ratio (V/C) is defined by

$$V/C = \frac{Hourly\ traffic\ volume}{Roadway\ capacity} \tag{1}$$

where V is the hourly traffic volume, and C is the allowable roadway capacity. The LoS of a roadway can be described with respect to the V/C ratios [7], as shown in Table 1.

Table 1. LoS indicator based on the V/C ratios.

LoS Class	Traffic State and Condition	V/C Ratio
A	Free flow	0–0.60
B	Stable flow with unaffected speed	0.61–0.70
C	Stable flow but speed is affected	0.71–0.80
D	High-density but stable flow	0.81–0.90
E	Traffic volume near or at capacity level with low speed	0.91–1.00
F	Breakdown flow	>1.00

The methods to calculate LoS vary with different constructions of roadways, such as freeways, multi-lane highways, two-lane highways, arterials, and intersections [21]. Although V/C is widely employed in measuring road traffic conditions, it is limited to measuring non-recurring congestion due to the uncertainty associated with the non-recurring congestion scenario. Since traffic conditions during an evacuation are associated with non-recurring congestion, the measurement must include uncertainty factors related to the disaster risk. Thus, the traffic volume during the evacuation under extreme weather can be redefined as

$$V(t) = (1 + \alpha)V_0(t) \tag{2}$$

where $V(t)$ is the hourly volume at time t during the evacuation period, V_0 is the average hourly volume at time t over the past years, and α is the scaling parameter. The value of α can be estimated by analyzing the average change in volume from previous years at

the same time. In this case, scaling parameters can account for traffic uncertainty during evacuation scenarios. This is because traffic measurement often has a known uncertainty associated with it. Thus, the traffic volume measurement during the evacuation can be scaled by α, which represents the uncertainty. In this way, the uncertainty can be propagated through calculations involving the scaled variable.

Moreover, the roadway capacity can also be affected due to lane closure, traffic accidents, or other potential damage during evacuation. The redefined road capacity can be written as

$$C(t) = (1 - \beta)C_0(t) \tag{3}$$

where $C(t)$ is the roadway capacity at time t during the evacuation period, $C_0(t)$ is the maximum roadway capacity during a normal traffic period, and β is the scaling parameter. The value of β can be estimated by analyzing current and historical data. Similar to the traffic volume during the evacuation, the roadway capacity measurement is often associated with known uncertainty. Thus, it can be scaled by β to ensure that the uncertainty can be propagated through calculations. Introducing the scaling parameters in Equations (2) and (3) into Equation (1) yields the updated V/C ratio as

$$\frac{V(t)}{C(t)} = \frac{(1 + \alpha)V_0(t)}{(1 - \beta)C_0(t)} \tag{4}$$

The calculation of α and β serves the purpose of capturing the relationship between $V(t)$ and $C(t)$ of the traffic performance. While it may initially appear that only $V(t)$ and $C(t)$ are sufficient for quantifying traffic resilience, the inclusion of α and β is crucial. These parameters enable a more comprehensive understanding of how well the system can handle traffic variabilities and uncertainties in the predicted traffic demand.

2.2. Augmented LSTM-Based Traffic Prediction

Numerous algorithms and frameworks have been developed for traffic prediction. In this paper, we adopt an augmented LSTM with the Kalman Filter approach (see Figure 2) to predict correlated and spatiotemporal traffic data and to account for model uncertainty. This framework is similar to the one proposed in ref. [24]. It is important to note that the proposed framework is not limited to LSTM-based algorithms; other traffic prediction algorithms could also be utilized to forecast future traffic conditions.

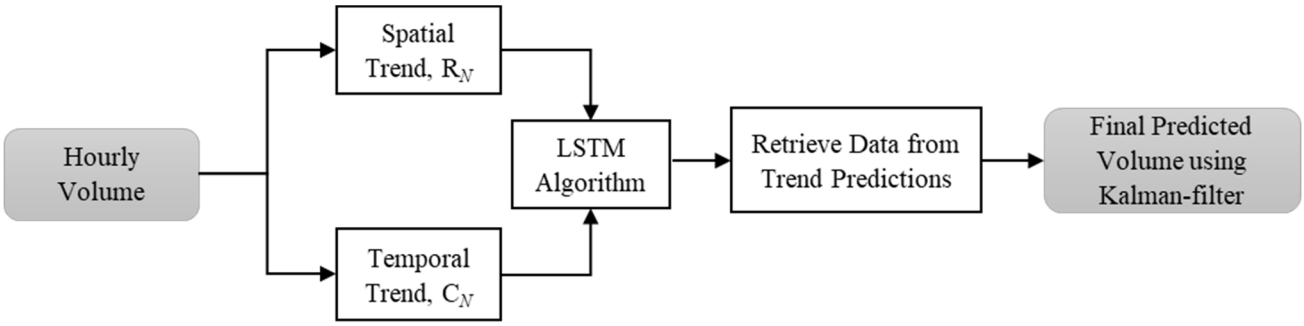

Figure 2. An augmented LSTM algorithm with Kalman Filter approach [24].

This LSTM-based algorithm uses a spatiotemporal traffic volume dataset to predict hourly volume over different traffic segments and routes. Initially, both spatial and temporal trends of the dataset are extracted and fed to the LSTM neural network to predict the trends separately. The details of the spatiotemporal data extraction process can be found in ref. [24]. Additionally, the architecture and details of a standard LSTM algorithm are detailed in refs. [25,26]. In short, the prediction of the standard LSTM algorithm can be formulated as:

$$\boldsymbol{i}_t = \sigma(\boldsymbol{W}_i[\boldsymbol{h}_{t-1}, \boldsymbol{x}_t] + \boldsymbol{b}_i) \tag{5}$$

$$f_t = \sigma\left(W_f[h_{t-1},\ x_t] + b_f\right) \tag{6}$$

$$\widetilde{c_t} = \tanh(W_c[h_{t-1},\ x_t] + b_c) \tag{7}$$

$$c_t = f_t \circ c_{t-1} + i_t \circ \widetilde{c_t} \tag{8}$$

$$o_t = \sigma(W_o[h_{t-1},\ x_t] + b_o) \tag{9}$$

$$h_t = o_t \circ \tanh(c_t) \tag{10}$$

where i_t is the input gate vector, f_t is the forget gate vector, and $\widetilde{c_t}$ is the input modulation vector for the memory cell. c_t, o_t, h_t, and x_t denote the memory cell vector, the output gate vector, the hidden state vector, and the input vector at time t. W_i, W_f, W_c, and W_o refer to the weight matrices for the input gate, forget gate, memory cell, and output gate. Similarly, b_i, b_f, b_c, and b_o are the bias vectors for the input gate, forget gate, memory cell, and output gate, respectively.

Sigmoid functions are typically used as the activation functions for all three gates (input gate i_t, forget gate f_t, and output gate o_t). The sigmoid function has an output value between 0 and 1, indicating no flow or a complete flow of information when activated. When the input gate i_t activates, the new input information is stored in the cell. i_t is obtained from the sigmoid function over the past hidden state vector h_{t-1}, the present input vector x_t, the weight matrix W_i, and the bias vector b_i. If the forget gate f_t is activated, the past cell state c_{t-1} will be forgotten. In this step, the decision is made on what information needs to be forgotten by using a sigmoid function over h_{t-1}, and x_t. The weight matrix for the forget gate is W_f, and the bias vector is b_f.

By using the activation function tanh over h_{t-1}, and x_t, an input modulation vector $\widetilde{c_t}$ can be calculated. The tanh function results in either positive or negative outputs, which refer to allowing an increase or decrease in the state. In this step, the weight matrix is W_c, and the bias vector is b_c. The new memory cell state is updated by multiplying the past state c_{t-1} by the forget gate f_t with the addition of the multiplication results from the input gate i_t with the modulation vector $\widetilde{c_t}$. The "$\circ$" denotes element-wise multiplication. The output gate o_t manages the propagation of the latest cell output c_t to the final state h_t, typically using a sigmoid activation function. In this step, the weight matrix is W_o, and the bias vector is b_o. The final state h_t also employs tanh as the activation function over the cell state c_t.

The prediction horizon or the length of time into the future that an augmented LSTM can accurately forecast depends on various factors, including the specific model architecture, the complexity of the data, and the training methodology. LSTM models, known for their ability to capture long-term dependencies, are particularly effective in handling time series data. In traffic studies, LSTM models have been successfully used to make accurate predictions several time steps or even several days into the future [27,28]. However, it is important to note that as the prediction horizon increases, the uncertainty and potential errors in the forecasts may also increase. To obtain the final volume predictions, the LSTM approach generates two sets of spatial and temporal predictions, which are then combined using the Kalman-filtering concept, as illustrated in Figure 2. Since the Kalman Filter approach has been extensively studied in the literature, this paper will not delve into its details. For interested readers, refs. [29,30] provide more comprehensive explanations.

LSTM is indeed powerful in capturing sequential dependencies and modeling complex patterns in traffic data. However, it is important to note that LSTM is not specifically designed for directly quantifying probabilities, particularly in the context of the parameters α and β that would be used in the quantification of traffic resilience. By considering both $V(t)$ and $C(t)$, and the parameters α and β, a more holistic assessment of traffic resilience can be achieved. This approach allows for the consideration of the variability in traffic volume

and the relationship between traffic volume and available capacity, providing a more accurate and comprehensive measure of the system's ability to handle traffic fluctuations and uncertainties.

2.3. Traffic Resilience Quantification

Resilience indexes in transportation system applications can be determined using varying performance metrics, for example, travel time, travel demand, capacity, reliability, and others [31]. This study defines the performance level based on the roadway's volume-to-capacity ratio or loss of service during the evacuation, as defined in Section 2.1. Road traffic performance during evacuation demonstrates a distinct trend compared to any other system performance, as shown in Figure 3.

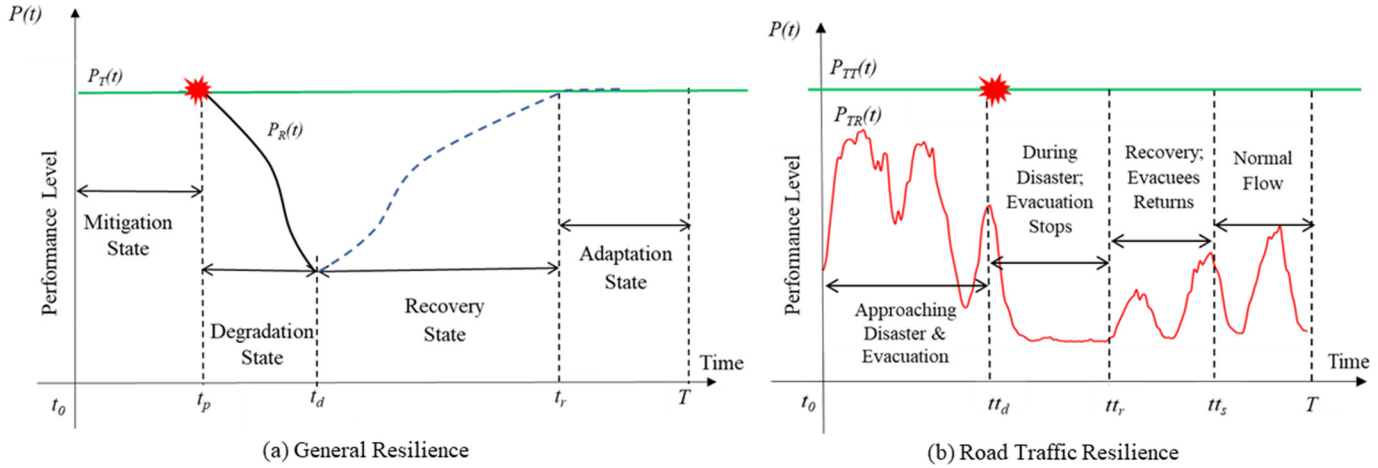

Figure 3. A comparison of trends between (**a**) general resilience curve and (**b**) road traffic resilience curve during an evacuation.

In the context of the resilience curve and concept (Figure 3a), the system's performance $P_R(t)$ undergoes a degradation phase after being exposed to a disruptive event at time t_p. This degradation is depicted as a decline in the resilience curve, indicating a decrease in the system's ability to maintain its desired level of performance. As the disaster propagates, the system's performance reaches a certain level, reflecting the impact and severity of the disruption. Following this degradation phase, the system enters the recovery state at time t_d, where efforts are made to restore and improve its performance. The recovery phase is represented by an upward trend in the resilience curve, illustrating the system's gradual recovery and return to its normal performance level by time t_r [32].

The resilience curve visually captures the dynamic behavior of the system's performance over time, highlighting the initial decline, the subsequent recovery process, and ultimately, the restoration of normal performance. On the contrary, the road traffic performance $P_{TR}(t)$ degrades (volume increases) long before the disaster occurs at time tt_d. As the evacuation process is in place following the disaster risk forecast to ensure the safety of the evacuees, a sudden increase in traffic volume is observed, causing congestion as a result of the road disturbance. The traffic volume decreases when a disaster is in progress because it is often not safe to travel when the hazard occurs. After the disaster period ends at time tt_r, the traffic flow further restores the normal trend as the evacuees start returning at time tt_s.

In the context of traffic resilience, the concept of the resilience curve can be related to non-recurring road traffic resilience. This curve defines the behavior of traffic resilience over different stages during a disaster event and evacuation process, as depicted in Figure 3b. The non-recurring road traffic resilience curve also consists of four distinct stages, each representing a specific phase of the disaster and evacuation scenario as follows:

- Stage 1: Approaching Disaster and Beginning of Evacuation. This stage marks the initial phase where the disaster is imminent and evacuation measures are initiated. Traffic conditions may start to deteriorate as the evacuation process begins;
- Stage 2: Ongoing Disaster; No Evacuation. The disaster is in full effect at this stage, and there is no ongoing evacuation. Traffic conditions may be severely impacted by the disaster, leading to disruptions and congestion on road networks;
- Stage 3: Recovery; Return of Evacuees. As the disaster subsides or the evacuation order is lifted, evacuees start returning to their homes or the affected areas. This stage represents the influx of traffic as people make their way back, potentially causing fluctuations and challenges in traffic flow;
- Stage 4: Regained Normal Traffic Flow. This final stage indicates the restoration of normal traffic conditions, where the road network recovers from the impact of the disaster, and traffic flow returns to pre-disaster levels.

Apart from the volatile traffic trend during the evacuation, the regular traffic data often shows a daily seasonality scenario. At the start of the day, traffic volume is usually low, which increases to the peak volume during peak hours, typically around 8:00 a.m. or 5:30 p.m. when people commute to and from work, and then decreases slowly towards the end of the day [7]. For a road segment, the daily traffic resilience cycle R_{Dn} can be quantified based on the general under-the-curve resilience metric as

$$R_{D1} = R_{D2} = \cdots R_{Dn} = \frac{\int_{t_0}^{T} P_{TR}\ (t)\ dt}{\int_{t_0}^{T} P_{TT}(t)\ dt} \tag{11}$$

$$P_{TR}\ (t) = 1 - \frac{V(t)}{C(t)} \tag{12}$$

where R_{Dn} is resilience at day cycle n. R_{Dn} is the ratio of the performance difference between the current traffic performance $P_{TR}(t)$ and the regular traffic trend $P_{TT}(t)$. t_o is the starting time of the study, typically at 12:00 a.m., and T is the end time considered in the study period, typically at 11:59 p.m. It should be noted that in Equation (11), the equal sign signifies that the equation is applicable to the calculation of daily traffic resilience for R_{D1}, R_{D2}, and R_{Dn}. However, it is important to acknowledge that the daily traffic performance PTR may vary, resulting in different levels of daily traffic resilience for R_{D1}, R_{D2}, and R_{Dn}. This implies that while the equation is the same, the specific values and outcomes of daily traffic resilience may differ based on the corresponding daily traffic performance. $P_{TT}(t)$ represents the anticipated or average traffic demand pattern during normal or non-disrupted conditions. It captures the inherent regularity or periodicity observed in the daily traffic data from time period t_o to T, typically spanning from 12:00 a.m. to 11:59 p.m. The value of $P_{TT}(t)$ is not necessarily fixed at one; rather, it is contingent upon the specific characteristics of the traffic data and the chosen normalization approach. In this research, historical data spanning two years is utilized to identify the recurring patterns and trends in traffic volume resulting from the disaster. By analyzing the traffic data over an extended duration, we can extract the regular traffic pattern, which serves as a benchmark for quantifying $P_{TT}(t)$.

The traffic resilience follows an upside-down general resilience curve in Figure 3a. Thus, the current traffic performance $P_{TR}(t)$ can be calculated as the maximum volume-to-capacity ratio minus the loss of service of a roadway, which is defined as the $V(t)/C(t)$ ratio, as shown in Equation (11). The value of 1 refers to the maximum volume-to-capacity ratio. The resilience of a given travel segment *Rsm* over a given timespan of a route can be calculated by combining all the daily resilience values of that particular segment, as illustrated in Figure 4. Thus, the travel segment resilience can be calculated as

$$R_{Sm} = Avg(R_{D1}, R_{D2}, \ldots, R_{Dn}) \tag{13}$$

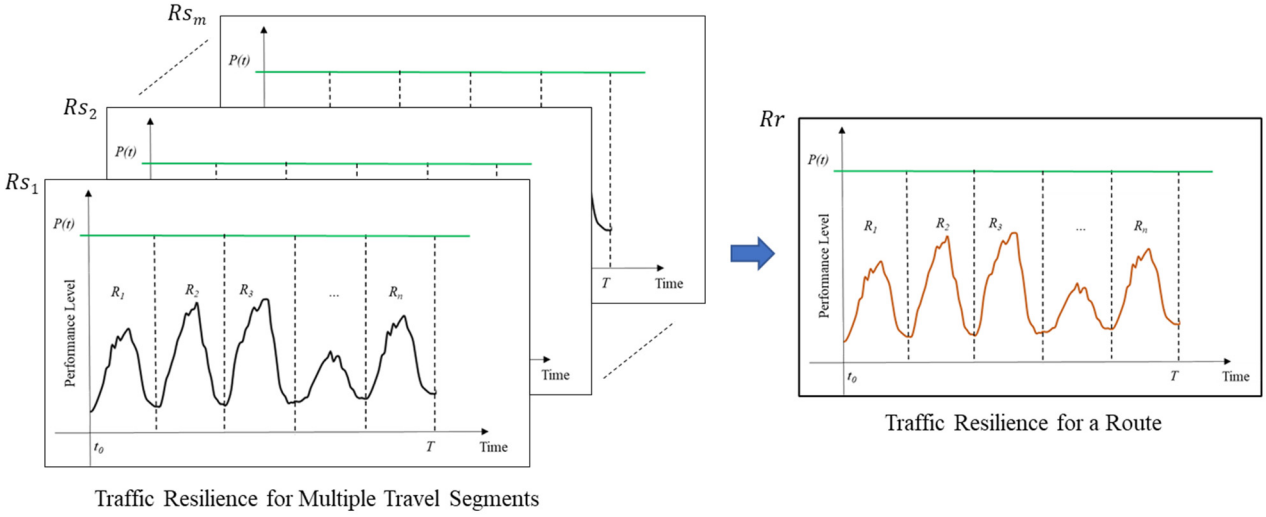

Figure 4. Traffic resilience quantification for a travel route.

A travel segment is defined as traveling from one stop station to the next, whereas a travel route comprises multiple segments throughout the day. To determine a route's traffic resilience over a timespan, all the resilience values from the associated segments need to be considered, as shown in Figure 4. The overall route traffic resilience R_r can be calculated by averaging all the segments' resilience,

$$R_r = Avg(R_{S1}, R_{S2}, \ldots R_{Sm}) \tag{14}$$

Monitoring the $V(t)/C(t)$ ratio under different conditions can assess an infrastructure's ability to cope with varying demand and capacity levels, and identify critical points that require attention to enhance its resilience. The $V(t)/C(t)$ ratio measures the performance and level of service of transportation infrastructure, but during extreme weather conditions, abrupt changes to this ratio can occur, and the ability to recover and restore pre-disaster performance becomes crucial. In this context, traffic resilience measures the transportation infrastructure's ability to adapt and recover from unexpected events that affect the $V(t)/C(t)$ ratio, rather than just maintaining a certain level of service [10]. To justify the use of $V(t)/C(t)$ ratio as a measure of traffic resilience, it is essential to understand that $V(t)/C(t)$ ratio is closely related to the transportation infrastructure's capacity and demand, which affects its ability to withstand disturbances. When the demand exceeds the transportation infrastructure's capacity, for example, during the evacuation process [11], the $V(t)/C(t)$ ratio increases, and the transportation infrastructure's performance deteriorates. Similarly, when the capacity exceeds the demand, the $V(t)/C(t)$ ratio decreases, and the transportation infrastructure's performance improves.

3. Case Study: Hurricane Irma

Hurricane Irma was selected because many studies and much information about it are available. A real-time traffic dataset during Hurricane Irma was obtained from the Florida Department of Transportation (FDOT) and used in this case study. The dataset is publicly accessible, and the information can be found in ref. [33].

3.1. Case Study Description

The traffic dataset used in the case study was collected during Hurricane Irma from 4 September 2017 to 15 September 2017, which includes various traffic parameters such as hourly vehicle volume around US I-75. These data were collected at different traffic monitoring stations along the US I-75 highway established by the FDOT. The study area considered in this paper includes ten stations (S1–S10) shown in Figure 5a, which are S1(0350), S2(0191), S3(9950), S4(9953), S5(0184), S6(0190), S7(0225), S8(0361), S9(0358),

and S10(0329). In this case study, each station is considered a travel segment, and the combination of all stations (or segments) is considered a travel route.

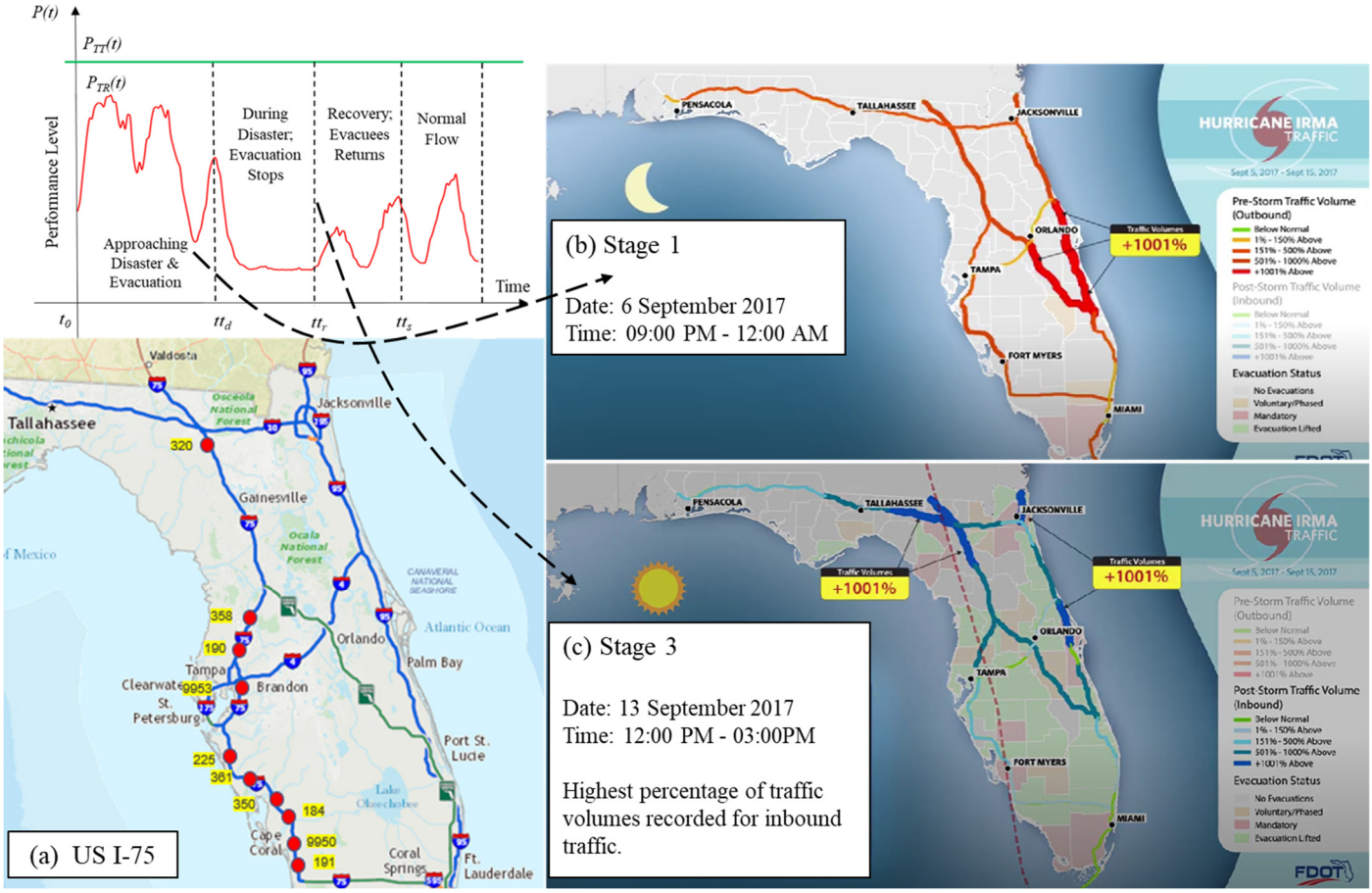

Figure 5. Overview of the case study (**a**) the study area along US I-75, (**b**) Stage 1—Traffic volume prior to Hurricane, during evacuation period on 6 September, 2017, and (**c**) Stage 3—Traffic volume post-Hurricane, evacuation lifted, and evacuee returns on 13 September 2017.

The dataset is separated into four traffic condition stages: Stage 1—Prior to the hurricane, during the evacuation period, outbound traffic (4 September 2017to 8 September 2017); Stage 2—During the hurricane (9 September 2017 and 10 September 2017); Stage 3—After the hurricane, evacuees returned, inbound traffic (11 September 2017 to 13 September 2017); and Stage 4—Normal traffic condition (14 September 2017 to 15 September 2017), as discussed in Section 2.3 and depicted in Figure 3b. During 4–8 September 2017, Category 4 Hurricane Irma approached slowly with a wind speed of 175 mph. The voluntary and mandatory evacuations occurred at this time, leading to a 501–1001% increase in volume, as shown in Figure 5b. As a result, major highways in Florida were congested, slowing the evacuation process for days. On 10 September 2017, Hurricane Irma's landfall occurred, and most Floridians had been evacuated, leaving the significant roads with very little to no traffic due to the severity of the hurricane; no travel was advised. During the post-storm period from 11 September 2017 to 13 September 2017, the residents started returning to their respective homes as the majority of mandatory evacuations were lifted. A high traffic density with an increase above +1001% was observed for some routes or road segments on 13 September 2017, as shown in Figure 5c.

As discussed in Section 2, the road traffic volume and capacity conditions with uncertainty factors were calculated with the equations introduced in Section 2.1. The spatial and temporal traffic data were then used for predicting spatial and temporal traffic trends with the augmented LSTM approach presented in Section 2.2. The augmented LSTM algorithm

was implemented to predict the post-storm traffic volume $V(t)$ over the route of US I-75, for all ten stations. Several experiments were performed with different combinations of hyperparameters to ensure the model's accuracy. The final and selected augmented LSTM architecture consisted of one 64-neuron LSTM layer, one flatten layer, and one dense layer. The adopted activation function was the tanh. The loss function adopted was the Adam optimizer with a mean squared error. For both temporal and spatial trend prediction, the same LSTM model was used.

With the predicted hourly volume $V(t)$, the road traffic performance $P_{TR}(t)$ was calculated for each of the stations using Equations (3) and (12). The uncertainty factor value α was determined from the predicted $V(t)$ for the post-storm period. The guide for highway capacity and operations analysis of active transportation and demand management strategies document released by the US Federal Highway Administration (FHWA) determined that the average capacity reduction of a freeway is 1.07% while the wind speed is above 10 and below or equal to 20 mph $(> 10 \leq 20$ mph) [34]. The value of the average capacity reduction also increases to 1.47% in the scenario where the wind speed is greater than 20 mph. Following this rule and the windspeed observation from Hurricane Irma, the uncertainty factor value β was set to 0.017 and 0.0147, depending on the wind speed.

The resilience curves for daily traffic condition $R_{D1}, R_{D2}, \ldots, R_{Dn}$ in a segment were measured with predicted data obtained from the LSTM and the segment resilience $R_{s1}, R_{s2}, \ldots, R_{sm}$ during the case study (period from 4–15 September 2017), was calculated from Equation (6). The route resilience value was further quantified from the average segment resilience, as shown in Equation (7).

3.2. Case Study Results

After implementing the proposed framework detailed in Section 2, the hourly volume prediction $V(t)$ for Station 1, S1(0350), is shown in Figure 6. The figure demonstrates the comparison plot of the actual data points and the predicted results for S1(0350). The post-storm hourly volume trend was predicted using the augmented LSTM framework, shown as the solid red line in Figure 6. The plot indicated that the augmented LSTM algorithm could successfully predict the post-storm recovery traffic condition with a relatively low mean absolute error of 39.312.

The hourly volume data of the given study period of 4–7 September 2017 was compared with the hourly volume data of 4–7 September from the past two years, 2015 and 2016, to find the uncertainty factor value of α over the study period. α values for S1(350) are shown in Figure 6b. The α values for S1(350) vary from -1 to 15.7. Over the evacuation period, the α value ranges from 0.3 on 4 September 2017, to 15.7 on 8 September 2017, and decreases in the next few days. During the hurricane period of 9–10 September, the α value ranges from 4.1 to -0.8. In the post-hurricane period of 11–15 September 2017, the α value increased, ranging from -0.6 to 0.6.

The α values can be either negative or positive, depending on the average change in hourly volume from the previous years' data. A positive α value indicates an increasing trend in hourly traffic volume, whereas a negative α value refers to decreasing hourly traffic activity compared to the previous data points. During the pre-storm evacuation period, the α value increases drastically because no evacuation activity occurred during the last years. This α value decreased to a negative value during the hurricane period due to a reduction in traffic activities on the same when compared to the previous years. The α value recovers post-hurricane as the evacuation stops and eventually converges with minor fluctuation when approaching the normal flow. The same prediction was conducted for the other nine segments, but the graphs from the nine segments are not presented in this section due to the page limitation.

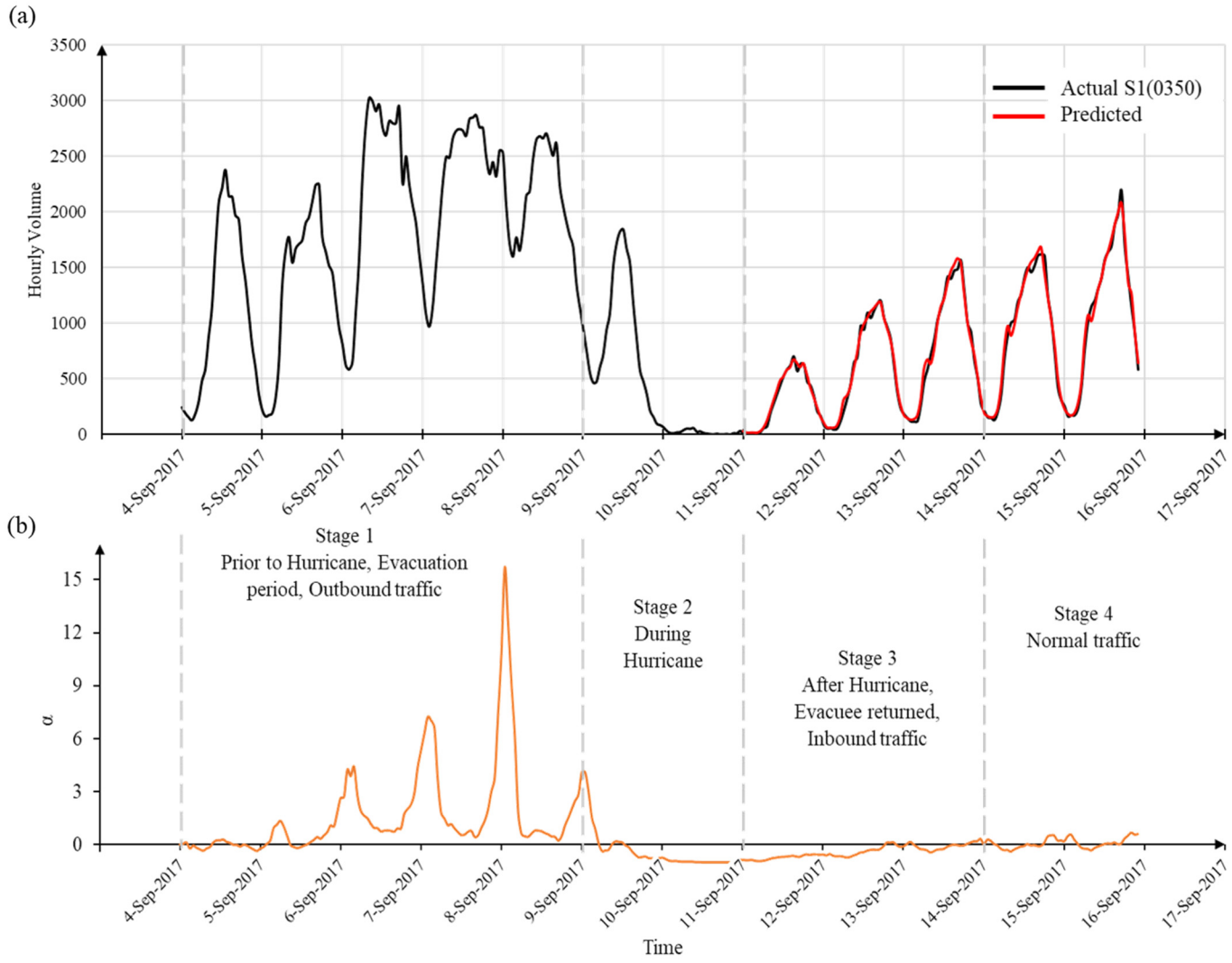

Figure 6. Prediction results for S1 (0350). (**a**) Actual data and prediction result of hourly volume; and (**b**) Change of α with time for S1(350) for S1(0350).

As mentioned in Section 2, the traffic performance shows a cyclic trend daily. The predicted traffic performances of all the segments $P_{TR}(t)$ were obtained using Equation (5), and the resilience curve for S1(0305) is shown in Figure 7a. The lowest traffic performances $P_{TR}(t)$ are observed over the pre-storm evacuation period of 4–9 September 2017. The traffic performance increased close to the targeted performance $P_{TT}(t)$, as there were hardly any vehicles during the hurricane. $P_{TR}(t)$ again reduced as the evacuees returned to their homes post-hurricane, before the traffic flow became normal at the final stage. The change in average traffic resilience along the US I-75 route is shown in Figure 7b, which mimics the general four-stage resilience curve in Figure 3a. These results can be further interpreted to mean that within the study period of 4–15 September 2017, the traffic infrastructures along US I-75 can be deemed resilient against traffic evacuation disturbances caused by Hurricane Irma.

Table 2 provides all the daily resilience values for each segment, the segment resilience, as well as the overall route resilience. For Segment 1 (S1), the daily traffic resilience on 4 September 2017 (prior to the hurricane) is found to be 0.834, and it is gradually reduced during the evacuation period, with the lowest resilience recorded being 0.738 on 8 September 2017. Another example is segment 3 (S3), which had the lowest daily traffic resilience recorded at 0.695 on 7 September 2017, two days prior to Hurricane Irma.

After 10 September 2017, the daily traffic resilience value for all segments recovered after Hurricane Irma.

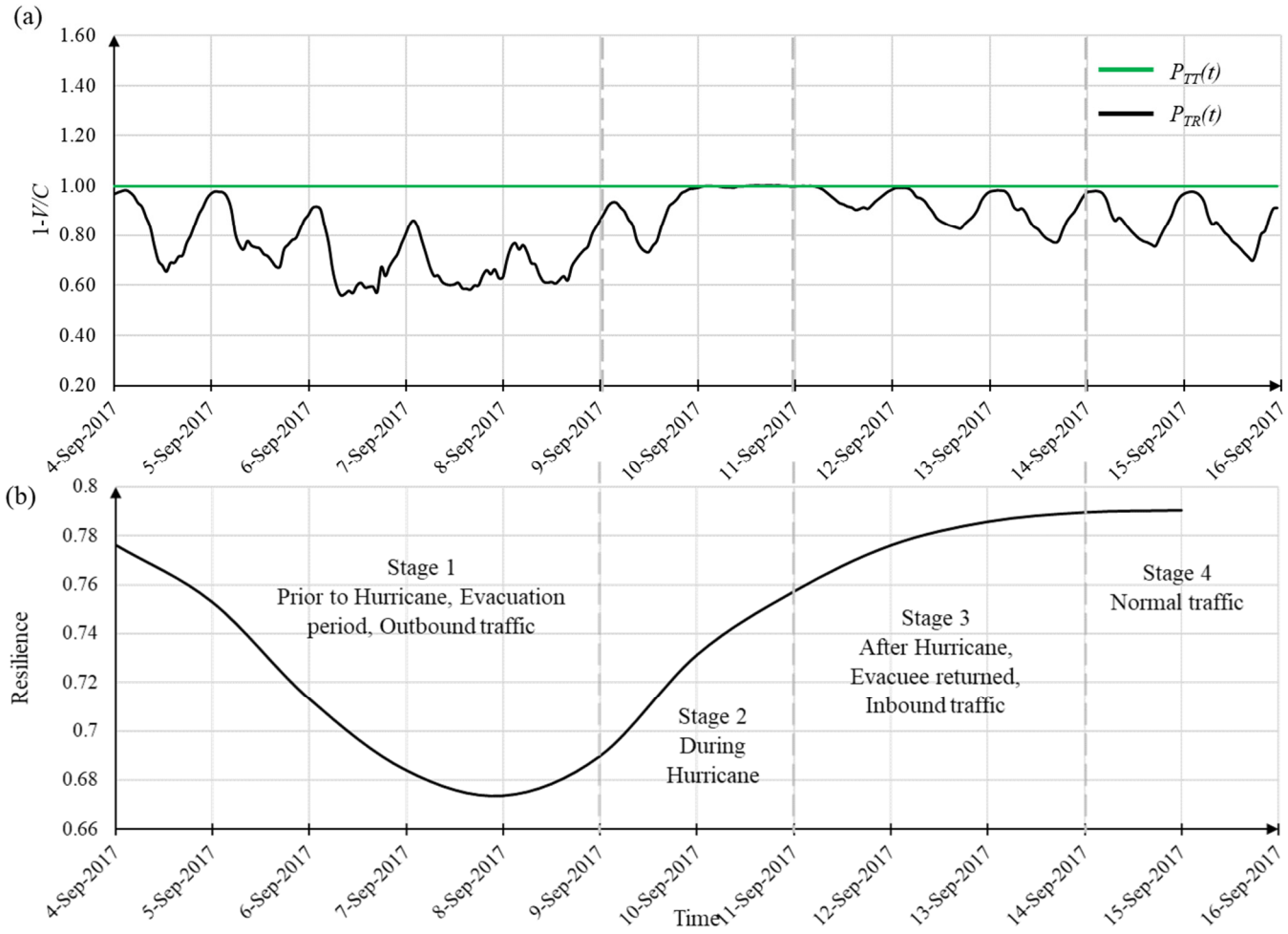

Figure 7. Traffic Resilience for (**a**) Segment S1(0350) and (**b**) US I-75 Route.

Table 2. Overall route resilience for US I-75 over ten stations.

			S1 (0350)	S2 (0191)	S3 (9950)	S4 (9953)	S5 (0184)	S6 (0190)	S7 (0225)	S8 (0361)	S9 (0358)	S10 (0320)
Daily traffic resilience	Stage 1	9 April 2017	0.834	0.814	0.782	0.609	0.780	0.744	0.726	0.826	0.839	0.811
		5 September 2017	0.821	0.785	0.740	0.567	0.734	0.721	0.686	0.802	0.842	0.834
		6 September 2017	0.776	0.764	0.711	0.528	0.690	0.677	0.652	0.749	0.813	0.773
		7 September 2017	0.750	0.747	0.695	0.504	0.672	0.643	0.624	0.719	0.791	0.697
		8 September 2017	0.738	0.755	0.705	0.491	0.680	0.614	0.613	0.707	0.767	0.667
	Stage 2	9 September 2017	0.760	0.788	0.745	0.512	0.721	0.610	0.639	0.732	0.746	0.644
		10 September 2017	0.794	0.819	0.781	0.577	0.761	0.659	0.689	0.770	0.776	0.688
	Stage 3	11 September 2017	0.814	0.833	0.799	0.613	0.781	0.694	0.718	0.793	0.802	0.725
		12 September 2017	0.825	0.841	0.809	0.640	0.797	0.722	0.740	0.811	0.822	0.755
		13 September 2017	0.831	0.846	0.814	0.650	0.806	0.736	0.749	0.820	0.834	0.774
	Stage 4	14 September 2017	0.834	0.847	0.814	0.649	0.809	0.742	0.749	0.824	0.842	0.788
		15 September 2017	0.835	0.845	0.812	0.645	0.809	0.744	0.747	0.826	0.847	0.797
Segment resilience			0.801	0.807	0.767	0.582	0.753	0.692	0.694	0.782	0.810	0.746
Route Resilience (S1-S10)			Min: 0.582 (S4), Avg: 0.676, Max: 0.810 (S9)									
Route Resilience (S6-S10)			Min: 0.692 (S6), Avg: 0.745, Max: 0.810 (S9)									

For each segment, the segment resilience values are obtained from the average daily traffic resilience during the study period of 4–17 September 2017. The segment resilience for Segment 1 (S1) is 0.801. The lowest segment resilience in the evacuation route from S1–S10 is found to be Segment 4 with 0.582, whereas the most resilient segment is Segment 9 with a 0.810 segment resilience value.

For travelers who trekked along the evacuation route, their route resilience was bounded by the lowest segment resilience. Considering a person who traveled the entire route from S1–S10, the route resilience is bounded by the least resilient segment (S4) and capped by the most resilient segment (S9), and the average route resilience is around 0.676 along S1–S10. This value can be further interpreted as follows: during the study period of 4–17 September 2017, the traffic condition along US I-75 was 67.6% resilient to the traffic evacuation disturbances posed by Hurricane Irma. For travelers who traveled only part of the evacuation route, for example, from S6–S10, the route resilience was bounded by the least resilient segment (S6), capped by the most resilient segment (S9), and the average route resilience was around 0.745 along S6–S10.

Similar concepts and interpretations can be applied to daily traffic route resilience, where the route resilience value is dependent mainly on the least resilient segment and may not be more resilient than the most resilient segment. These results show that the response uncertainty of the travelers was considered when interpreting the route resilience. Please note that the resilience value obtained does not represent the traffic conditions entirely, or the transportation infrastructure in Florida.

4. Further Discussion and Future Work

The framework implemented in this paper is a novel approach to determining traffic resilience. The proposed integrated predictive resilience framework defines the traffic resilience of route US I-75 based on the predicted traffic volume during Hurricane Irma. As traffic data demonstrates a cyclic trend, implementing a conventional resilience quantification approach might not be sufficient to evaluate the traffic resilience of a roadway. To overcome this challenge, the proposed framework quantifies the daily and associated segments' resilience to compute the overall route resilience. Moreover, the proposed framework adopts a modified *V/C* to define roadway performance by introducing uncertainty factors. The modified *V/C* can capture the uncertainty in traffic conditions due to extreme weather that are often not considered in the regular *V/C* metric in Equation (1).

Note that the resilience value obtained may vary with several factors, such as the scope of the study period, study area, resilience performance indicator, and prediction algorithm. The resilience concept fundamentally depends on time [35]. If the study period is shortened or lengthened, this may affect the resilience values obtained for the traffic segments and routes. The case study presented only includes ten stations that make up a portion of US I-75. These ten segments cover the area under mandatory or voluntary evacuation orders, but do not represent the entire US I-75. Due to the limited data obtained, other traffic routes were not considered in the case study. Suppose the study area was expanded to include more traffic routes, for example, interstates US I-4 or US I-95 and other local highways; in that case, the resilience values for the routes would be expected to change. Additionally, segment resilience would need to be recalculated for the segments associated with that route. The presented segment resilience in this case study is only valid for the US I-75 route under evacuation orders.

As mentioned in ref. [31], various performance indicators can be used as a resilience index in the transportation system. This paper focuses on a roadway's loss of service, which can be quantified with a volume-to-capacity (*V/C*) ratio. The resilience value will change if another performance indicator is implemented, such as travel time or demand. Moreover, since this paper focuses on the predicted resilience value, the data-driven algorithm used to perform the prediction may alter the resilience value. The inherent nature of the prediction algorithm may not always result in the same prediction value based on the input data [36]. In traffic applications, the fundamental LSTM algorithm can be

enhanced in conjunction with other methods, such as optimization-based decision-making, and may offer several advantages [37,38]. These combinations may improve efficiency by finding optimal solutions and optimizing decision-making processes. Data processing for training the algorithm may also affect the predicted value, and this will be studied further in the future.

In the future, this study will also incorporate references to studies conducted in different countries or continents, such as Australia [37] or Africa [8], to ensure that the significance of this research can be further emphasized. This approach will broaden the scope of this study, showcasing its relevance and applicability beyond specific regions or events. It will demonstrate the transferability of findings and highlight the global relevance of addressing traffic resilience in disaster management. Additionally, referencing studies from different contexts enhances the overall knowledge base and provides a comprehensive understanding of the subject matter, contributing to advancing research in this field.

Although the proposed integrated data-driven framework approach can predict various levels of traffic resilience, one drawback is that the prediction of traffic volumes does not consider future weather data. In the future, the framework will be improved by implementing weather datasets to provide a more comprehensive overview of the impact of weather on traffic resilience. Lastly, the proposed framework will be implemented to access traffic resilience assessments of past hurricane scenarios before being implemented for future hurricane scenarios. Additionally, the integrated data-driven predictive resilience framework will be adopted for different disaster scenarios, such as wildfires and major flooding.

5. Conclusions

This study proposed an integrated data-driven resilience framework for predicting traffic resilience during a disaster while considering multiple sources of uncertainty: data, model, and response uncertainty. The proposed framework adopts the augmented LSTM with the Kalman Filter framework to forecast traffic conditions. A real-time traffic dataset collected during Hurricane Irma is employed to demonstrate the effectiveness of the proposed framework. Before predicting traffic performance, uncertainty factors that account for data uncertainty are introduced in measuring the current traffic condition. A four-stage traffic evacuation scenario is considered, which includes the pre-storm evacuation, during the hurricane, the post-storm evacuee return, and the recovered normal traffic condition period. For the post-storm and recovered periods, the traffic conditions were predicted based on earlier evacuation traffic data. The prediction results revealed that a modified roadway traffic resilience quantification approach was capable of quantifying various levels of traffic resilience. From the prediction results, the daily, segment, and finally, the overall route resilience were quantified by considering the response uncertainty from the travelers. The behavior obtained for the route resilience mimics the general resilience curve. The proposed framework overcomes the challenges of incorporating uncertainty into evaluating traffic conditions and resilience. By implementing the proposed framework, the traffic resilience of a roadway can be predicted, which can further help in decision-making for more disaster-resilient transportation infrastructures. The broader impact of this study is essential for effective emergency management and can lead to better outcomes for people and communities affected by these adverse and often inevitable events.

Author Contributions: Conceptualization, T.A. and N.Y.; methodology, T.A., L.G.A., Z.L. and N.Y.; software, T.A.; validation, T.A., L.G.A., Z.L. and N.Y.; formal analysis, T.A. and N.Y.; investigation, T.A and L.G.A.; resources, N.Y.; data curation, T.A.; writing—original draft preparation, T.A. and N.Y.; writing—review and editing, Z.L. and L.G.A.; visualization, T.A. and N.Y.; supervision, L.G.A., Z.L. and N.Y.; project administration, N.Y.; funding acquisition, N.Y. All authors have read and agreed to the published version of the manuscript.

Funding: This research was partially funded by the National Science Foundation (NSF) EPSCoR RII Track-2 Program under the NSF award # OIA-2119691.

Institutional Review Board Statement: Not applicable.

Informed Consent Statement: Not applicable.

Data Availability Statement: Data is available upon request.

Acknowledgments: This research was made possible through a grant from the National Science Foundation (NSF) and data from the Florida Department of Transportation (FDOT). The findings and opinions presented in this manuscript are those of the authors only and do not necessarily reflect the perspective of the sponsors.

Conflicts of Interest: The authors declare no conflict of interest.

References

1. National Research Council; Division on Engineering and Physical Sciences; Computer Science and Telecommunications Board; Committee on Using Information Technology to Enhance Disaster Management. *Improving Disaster Management: The Role of IT in Mitigation, Preparedness, Response, and Recovery*; Rao, R.R., Eisenberg, J., Schmitt, T., Eds.; National Academies Press: Washington, DC, USA, 2007.
2. Berkoune, D.; Renaud, J.; Rekik, M.; Ruiz, A. Transportation in disaster response operations. *Socio-Econ. Plan. Sci.* **2012**, *46*, 23–32. [CrossRef]
3. Mahmood, Y.; Afrin, T.; Huang, Y.; Yodo, N. Sustainable Development for Oil and Gas Infrastructure from Risk, Reliability, and Resilience Perspectives. *Sustainability* **2023**, *15*, 4953. [CrossRef]
4. Afrin, T.; Yodo, N. A Hybrid Recovery Strategy toward Sustainable Infrastructure Systems. *J. Infrastruct. Syst.* **2022**, *28*, 04021054. [CrossRef]
5. Rahman, M.M.; Afrina, T.; Scully, E.; Yodo, N. Two-Echelon Cooperative Vehicle and UAV Routing for Last Mile Humanitarian Relief Operations. In Proceedings of the IISE Annual Conference and Expo 2022, Seattle, WA, USA, 21–24 May 2022; pp. 1–6.
6. Faturechi, R.; Miller-Hooks, E. Measuring the performance of transportation infrastructure systems in disasters: A comprehensive review. *J. Infrastruct. Syst.* **2015**, *21*, 04014025. [CrossRef]
7. Afrin, T.; Yodo, N. A survey of road traffic congestion measures towards a sustainable and resilient transportation system. *Sustainability* **2020**, *12*, 4660. [CrossRef]
8. Fraser, M.S.; Wachira, B.W.; Flaxman, A.D.; Lee, A.Y.; Duber, H.C. Impact of traffic, poverty and facility ownership on travel time to emergency care in Nairobi, Kenya. *Afr. J. Emerg. Med.* **2020**, *10*, 40–45. [CrossRef]
9. Nogal, M.; O'Connor, A.; Caulfield, B.; Martinez-Pastor, B. Resilience of traffic networks: From perturbation to recovery via a dynamic restricted equilibrium model. *Reliab. Eng. Syst. Saf.* **2016**, *156*, 84–96. [CrossRef]
10. Calvert, S.C.; Snelder, M. A methodology for road traffic resilience analysis and review of related concepts. *Transp. A Transp. Sci.* **2018**, *14*, 130–154. [CrossRef]
11. Zhang, Z.; Liu, Y.; Tong, Q.; Guo, S.; Li, D. Evacuation based on spatio-temporal resilience with variable traffic demand. *J. Manag. Sci. Eng.* **2021**, *6*, 86–98. [CrossRef]
12. Abudayyeh, D.; Nicholson, A.; Ngoduy, D. Traffic signal optimisation in disrupted networks, to improve resilience and sustainability. *Travel Behav. Soc.* **2021**, *22*, 117–128. [CrossRef]
13. Yao, K.; Chen, S. Resilience-based adaptive traffic signal strategy against disruption at single intersection. *J. Transp. Eng. Part A Syst.* **2022**, *148*, 04022018. [CrossRef]
14. Akhtar, M.; Moridpour, S. A review of traffic congestion prediction using artificial intelligence. *J. Adv. Transp.* **2021**, *2021*, 8878011. [CrossRef]
15. Roy, K.C.; Hasan, S.; Culotta, A.; Eluru, N. Predicting traffic demand during hurricane evacuation using Real-time data from transportation systems and social media. *Transp. Res. Part C Emerg. Technol.* **2021**, *131*, 103339. [CrossRef]
16. Rahman, R.; Hasan, S. Short-term traffic speed prediction for freeways during hurricane evacuation: A deep learning approach. In Proceedings of the 2018 21st International Conference on Intelligent Transportation Systems (ITSC), Maui, HI, USA, 4–7 November 2018; pp. 1291–1296.
17. Rahman, R.; Hasan, S. A Deep Learning Approach for Network-wide Dynamic Traffic Prediction during Hurricane Evacuation. *arXiv* **2022**, arXiv:2202.12505. [CrossRef]
18. Dey, A.; Yodo, N. Robust Response Surface Optimization under Model Parameter Uncertainty. In Proceedings of the IISE Annual Conference and Expo 2021, Montreal, QC, Canada, 22–25 May 2021; pp. 908–913.
19. Jiang, Y.; Yuan, Y. Emergency logistics in a large-scale disaster context: Achievements and challenges. *Int. J. Environ. Res. Public Health* **2019**, *16*, 779. [CrossRef]
20. Sherstinsky, A. Fundamentals of recurrent neural network (RNN) and long short-term memory (LSTM) network. *Phys. D Nonlinear Phenom.* **2020**, *404*, 132306. [CrossRef]
21. *Highway Capacity Manual*; Transportation Research Board Special Report 209; National Research Council: Washington, DC, USA, 1994.
22. Wan, C.; Yang, Z.; Zhang, D.; Yan, X.; Fan, S. Resilience in transportation systems: A systematic review and future directions. *Transp. Rev.* **2018**, *38*, 479–498. [CrossRef]

23. Tang, J.; Heinimann, H.R. A resilience-oriented approach for quantitatively assessing recurrent spatial-temporal congestion on urban roads. *PLoS ONE* **2018**, *13*, e0190616. [CrossRef]
24. Afrin, T.; Yodo, N. A Long Short-Term Memory-based correlated traffic data prediction framework. *Knowl.-Based Syst.* **2022**, *237*, 107755. [CrossRef]
25. Hochreiter, S.; Schmidhuber, J. Long short-term memory. *Neural Comput.* **1997**, *9*, 1735–1780. [CrossRef]
26. Olah, C. Understanding LSTM Networks. 2015. Available online: https://colah.github.io/posts/2015-08-Understanding-LSTMs/ (accessed on 15 August 2022).
27. Wang, Z.; Su, X.; Ding, Z. Long-term traffic prediction based on lstm encoder-decoder architecture. *IEEE Trans. Intell. Transp. Syst.* **2020**, *22*, 6561–6571. [CrossRef]
28. Ma, X.; Tao, Z.; Wang, Y.; Yu, H.; Wang, Y. Long short-term memory neural network for traffic speed prediction using remote microwave sensor data. *Transp. Res. Part C Emerg. Technol.* **2015**, *54*, 187–197. [CrossRef]
29. Pérez-Ortiz, J.A.; Gers, F.A.; Eck, D.; Schmidhuber, J. Kalman filters improve LSTM network performance in problems unsolvable by traditional recurrent nets. *Neural Netw.* **2003**, *16*, 241–250. [CrossRef] [PubMed]
30. Welch, G.; Bishop, G. An Introduction to the Kalman Filter. 1995. Available online: https://www.cs.unc.edu/~welch/media/pdf/kalman_intro.pdf (accessed on 15 August 2022).
31. Ahmed, S.; Dey, K. Resilience modeling concepts in transportation systems: A comprehensive review based on mode, and modeling techniques. *J. Infrastruct. Preserv. Resil.* **2020**, *1*, 8. [CrossRef]
32. Yodo, N.; Wang, P. Engineering resilience quantification and system design implications: A literature survey. *J. Mech. Des.* **2016**, *138*, 111408. [CrossRef]
33. Florida Department of Transportation (FDOT). Traffic Data. Available online: https://www.fdot.gov/statistics/trafficdata/default.shtm (accessed on 15 August 2022).
34. Dowling, R.G.; Margiotta, R.A.; Cohen, H.; Skabardonis, A. *Guide for Highway Capacity and Operations Analysis of Active Transportation and Demand Management Strategies*; No. FHWA-HOP-13-042; Federal Highway Administration, Office of Operations: Washington, DC, USA, 2013; Available online: https://ops.fhwa.dot.gov/publications/fhwahop13042/fhwahop13042.pdf (accessed on 15 August 2022).
35. Yodo, N.; Wang, P.; Zhou, Z. Predictive resilience analysis of complex systems using dynamic Bayesian networks. *IEEE Trans. Reliab.* **2017**, *66*, 761–770. [CrossRef]
36. Walker, W.E.; Harremoës, P.; Rotmans, J.; Van Der Sluijs, J.P.; Van Asselt, M.B.; Janssen, P.; Krayer von Krauss, M.P. Defining uncertainty: A conceptual basis for uncertainty management in model-based decision support. *Integr. Assess.* **2003**, *4*, 5–17. [CrossRef]
37. Yazdani, M.; Haghani, M. Elderly people evacuation planning in response to extreme flood events using optimisation-based decision-making systems: A case study in western Sydney, Australia. *Knowl.-Based Syst.* **2023**, *274*, 110629. [CrossRef]
38. Liu, Y.Y. Multi-Objective Optimization on Dynamic Complex Networks. Ph.D. Thesis, The University of Manitoba, Winnipeg, MB, Canada, 2022.